Ion Scattering Spectrometry

R. J. MacDonald

Department of Physics, Australian National University; present address:
Department of Physics, University of Newcastle, N.S.W. 2308.

Abstract

The scattering of ions from the surface and near surface region is a common method of analysing solid surfaces. The basic principles of ion scattering spectrometry are reviewed with emphasis on those factors which affect the interpretation of the scattering measurements. In particular we emphasize the role of the interatomic potential and the neutralization factor involved in ion–surface scattering. Several aspects of ion scattering spectrometry are then outlined, including its application to studies of the composition and crystallographic structure of surfaces. Some factors of ion scattering spectrometry peculiar to surfaces are mentioned, e.g. the sequential 'double' collision event. The use of photon emission studies as a means of inferring something of the neutralization processes involved is briefly outlined, emphasizing the study of polarized emission from scattered ions at glancing incidence to the target surface.

1. Introduction

Consider an ion beam of mass M_1 and energy E_0 incident on a surface consisting of atoms of mass M_2. The ions are scattered from the target atom through an angle θ, where they are energy analysed and detected by a suitable system. Provided that the angle of incidence to the surface, measured from the surface normal, is not too large, some ions will suffer a binary collision event, and their scattered energy E_1 will, from conservation of energy and momentum, be given by

$$\frac{E_1}{E_0} = \frac{M_1^2}{(M_1+M_2)^2}\left[\cos\theta \pm \left\{\left(\frac{M_1}{M_2}\right)^2 - \sin^2\theta\right\}^{\frac{1}{2}}\right]^2. \tag{1}$$

The scattered energy E_1 from this binary collision event is independent of the interaction potential, but the number of scattered ions depends on the interaction potential through the differential cross section for scattering.

The experimental situation is shown schematically in Fig. 1*a*. Ions scattered from the surface are analysed by an energy dispersive device at some angle θ. The device used depends on the energy of the scattered ions. At low energies electrostatic or magnetic devices may be used, and at higher energies solid state detectors provide the best means of analysis. Some particles will be scattered from atoms M_2, located at a depth x below the surface. These ions will lose energy due to small angle (large impact parameter) elastic collisions and to inelastic processes (electron excitation) inside the target. The energy E_1' will be thus reduced below the value for ions scattered from the surface, and

$$E_1' = k\left(E_0 - \frac{x}{\cos\alpha}\frac{\mathrm{d}E}{\mathrm{d}x}\right) - \frac{x}{\cos(\theta-\alpha)}\frac{\mathrm{d}E}{\mathrm{d}x}, \tag{2}$$
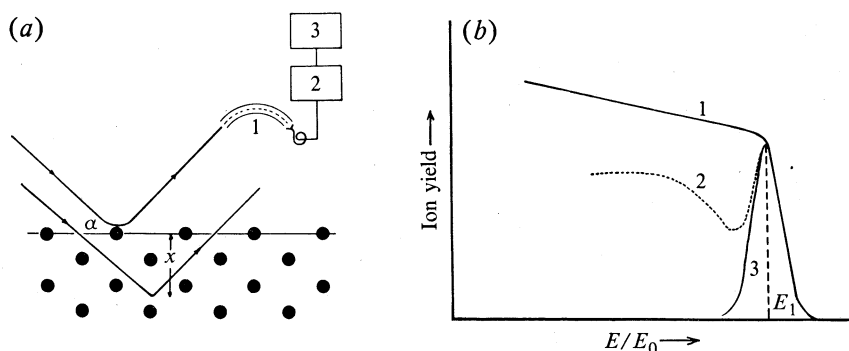
Fig. 1. (a) Schematic representation of the experimental arrangement. Ions incident at angle α are scattered into a detector: 1, energy analyser and detector; 2, pulse amplification and shaping; 3, data storage. (b) Schematic representation of the energy spectrum of scattered particles: 1, typical of high energy ions; 2, typical of medium energy ions; 3, typical of low energy ions.

where k is the right-hand side of equation (1) and α is the angle of incidence. The resultant energy spectrum is shown schematically in Fig. 1b. At all energies there is a sharp cutoff at energy E_1 corresponding to the ions scattered from the surface and the energy spectrum extends then to lower energies, the form of the extension depending on the energy of the incident ions. At low energies almost all ions penetrating below the surface are neutralized and not detected in the usual analysing apparatus. At intermediate energies a 'surface' peak is readily distinguishable and there exists a tail of particles scattered at lower energies from beneath the surface. At high energies for a polycrystalline target, a surface peak is not distinguishable and a broad spectrum extending to low energies is observed. The division into low, intermediate and high energies depends mainly on the ion velocity and the ratio M_2/M_1.

The idealized situation would assume that all particles scattered through the angle θ are detectable. At the higher energy region for light ions (i.e. H^+ and He^+), where the incident ion energy exceeds say 10^5 eV, this assumption is reasonable since the type of detector normally used for these particles detects both charged and neutral particles equally well. Further, the charged fraction of such scattered ions is high. At low energies (10^4 eV or less) the detectors used to provide energy analysis usually depend on the particle being charged (e.g. electrostatic or magnetic analysers) and so only those incident ions which survive the interaction with a solid still in a charged state need be considered. At energies less than 10^4 eV, for all incident ions, neutralization events are very important and in general incident ions with energies less than about 2 keV will only survive the interaction with a clean surface in a charged state if they are scattered from the surface layer itself. Those ions penetrating below the surface and suffering a large angle scattering event through θ, have an extremely high probability of emerging from the surface as a neutral atom. Thus low energy ion scattering (LEIS) provides a means of measuring the surface composition at very low adsorbate or contaminate coverage. An example of this type of spectrum is shown in Fig. 2a for the case of 1 keV He^+ ions scattered through 90° from an Ni target which has been previously cleaned by bombardment with 2 keV Ne^+ ions, and subsequently annealed. As the surface is contaminated, the adsorbed atoms shadow the underlying surface atoms, reducing the signal from the substrate (Ni) atom and in-

creasing the signal from the adsorbate. This is shown in Fig. 2b for 1 keV He^+ scattered from an Ni target covered with an equilibrium (~ 0.5 monolayer) coverage of CO.

Some experimental studies of neutral scattered particles have been made. These usually involve the use of stripping cells to ionize the neutrals which are detected by a charged particle analyser, or the use of time of flight spectrometers (Bhattacharya *et al.* 1980; Luitjens *et al.* 1980). Some results of the measurements of Bhattacharya
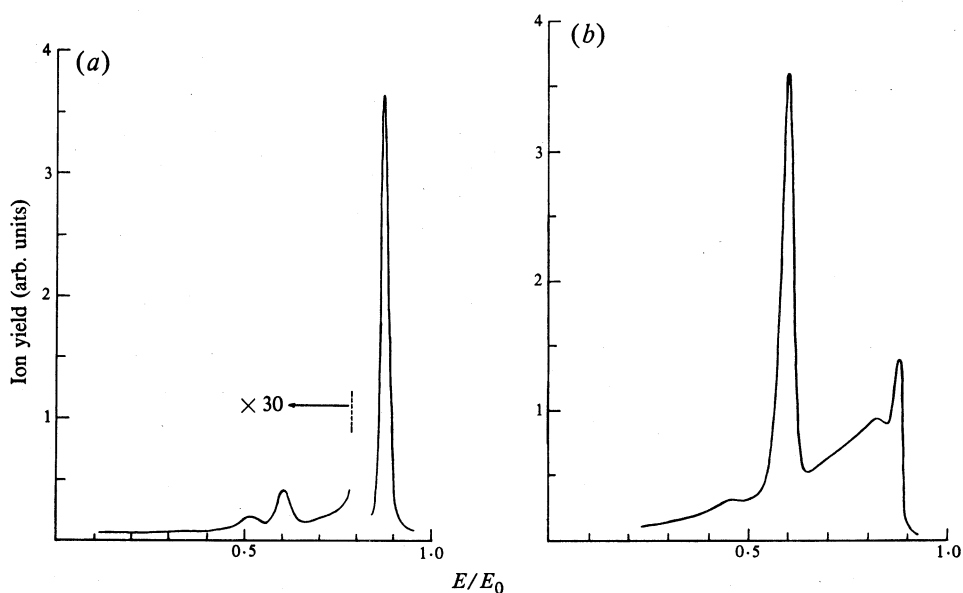

Fig. 2. Energy spectrum of 1 keV He^+ ions scattered through an angle of $\theta = 90°$ from (*a*) an Ni surface cleaned by ion bombardment and annealing, and (*b*) an Ni surface with an equilibrium coverage of CO adsorbed. The yield scale in (*b*) is a factor of 10 smaller than that of (*a*).

et al. (1980) are shown in Fig. 3. These results show the existence of a surface scattering peak in the charged fraction yield as a function of the incident ion energy. The charged fraction resulting from ions scattered from below the surface falls on a universal curve which shows an increasing ionized component as the exit energy increases. If the curve is plotted as a function of velocity rather than energy, it is found for example that the charged fraction of H^+ scattered as a result of H_2^+ incident on the same target follows the He^+ result very closely. The H^+ line in Fig. 3 demonstrates this result.

This paper will concentrate on the scattering of low energy ions (10^4 eV or less) from surfaces, on the use of these scattered ions in studies of surface composition and structure, and on the physics of the scattering event. For an ion beam of energy E_0 incident on a surface and with the analyser set to detect and energy analyse the scattered ions at a scattering angle θ, the signal due to scattering of ions of mass M_1 from atoms of mass M_2 is given by

$$I = I_0 N_i (d\sigma/dE_1) f(E_1) d\Omega,\tag{3}$$

where I_0 is the incident ion beam intensity (ions per unit area), N_i is the target atom density (atoms per unit area), and $d\sigma/dE_1$ is the differential cross section for scattering of ions into the energy range dE_1 at E_1 and corresponds to the differential cross section for scattering of ions into the angle $d\theta$ at θ. Further, $d\Omega$ is the solid angle of the detector and $f(E_1)$ represents the neutralization factor for ions scattered through θ.
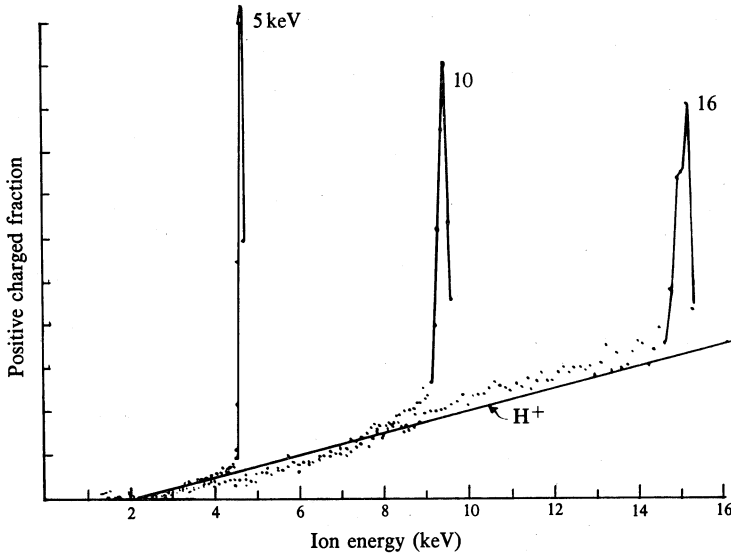

Fig. 3. Positive charged fraction yield for 5, 10 and 16 keV He$^+$ ions scattered at an angle of $\theta = 135°$ from the surface of an Au target. The H$^+$ line represents the charged fraction of H$^+$ ions scattered from Au at $\theta = 135°$, at points of equal velocity to the He$^+$ ions (after Bhattacharya *et al.* 1980).

The differential cross section depends on the interaction potential. In Section 2 we discuss our understanding of this function. The neutralization factor is one parameter which is not well understood; it depends on a variety of parameters such as the ion velocity relative to the surface, the ion–target combination, the state of the surface, and so on. We will discuss this factor in more detail in Section 3.

2. The Interaction Potential

The number of ions scattered into an angular range $d\theta$ at θ depends on the interaction potential between the incident ion and the target atom. In all the scattering studies discussed here, the incident ion energy is some hundreds of eV or more, and so there is considerable orbital interaction, and the potential may be considered to be purely repulsive. At high energies, such that the incident ion penetrates the innermost electron orbitals, the nucleus is unscreened and the Coulomb potential applies. The Rutherford scattering cross section is then applicable. For light ions, this involves incident ion energies of 10^5 eV and higher.

At lower energies, the incident ion is screened from the nucleus of the struck particle by the electron distribution. The potential is then of the form of the Bohr or screened Coulomb potential

$$V(r) = C(Z_1 Z_2 e^2/r)\, \phi(r/a)\,, \tag{4}$$

where Z_1 and Z_2 are the atomic numbers of the incident and struck particles respectively, e is the electronic charge, r the interatomic spacing and $\phi(r/a)$ the screening function. The constant C is dictated principally by the choice of units. The screening radius a is a function of the collision partners and is usually expressed in the form

$$a = f(Z_1, Z_2) a_0, \qquad (5)$$
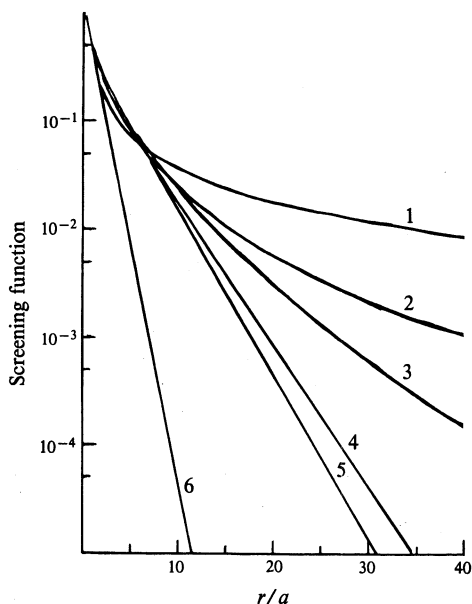
where a_0 is the Bohr radius for hydrogen.

Fig. 4. Variation of several popular screening functions as a function of the interatomic spacing r in units of screening radii a: 1, inverse square; 2, Latter; 3, Roberts; 4, Moliere; 5, Csavinsky; 6, Bohr (after O'Connor 1978).

Much has been written about the interatomic potential and the forms of the screening function (Torrens 1972). The screening function can be calculated or developed empirically. Some commonly used forms are shown in Fig. 4. In the experiments involved in ion–surface scattering, the r/a values of most importance are in the range $0 \cdot 1$–5, particularly if the experiments involve low to medium energy ions. Differences in the values of the screening function thus tend not to be important, because the work is mainly qualitative and, as we will see, uncertainties regarding the level of neutralization of the scattered ion greatly exceed uncertainties regarding the screening function. The form of the interatomic potential is important in understanding the general behaviour of the scattering process. Actual values of the potential are important because much of the interpretation of experimental results, particularly when single crystals are involved, is aided by concurrent computer simulation of the scattering event. There is some information about the potential that we can gain from ion–surface scattering experiments, and some experiments along these lines will be discussed later in Section 4.

3. Neutralization

The processes responsible for the neutralization of the scattered ions are the most important unknown quantity in the application of ion scattering to studies of surfaces.

Much of the work on neutralization in ion–surface scattering uses the specific models involving electron exchange processes between ions and surfaces proposed by early workers such as Massey (1930), Cobas and Lamb (1944) and Shekhter (1937), and discussed in detail by Hagstrum (1954) in his work on ion neutralization spectroscopy. The main processes are shown schematically in Fig. 5, involving resonance and
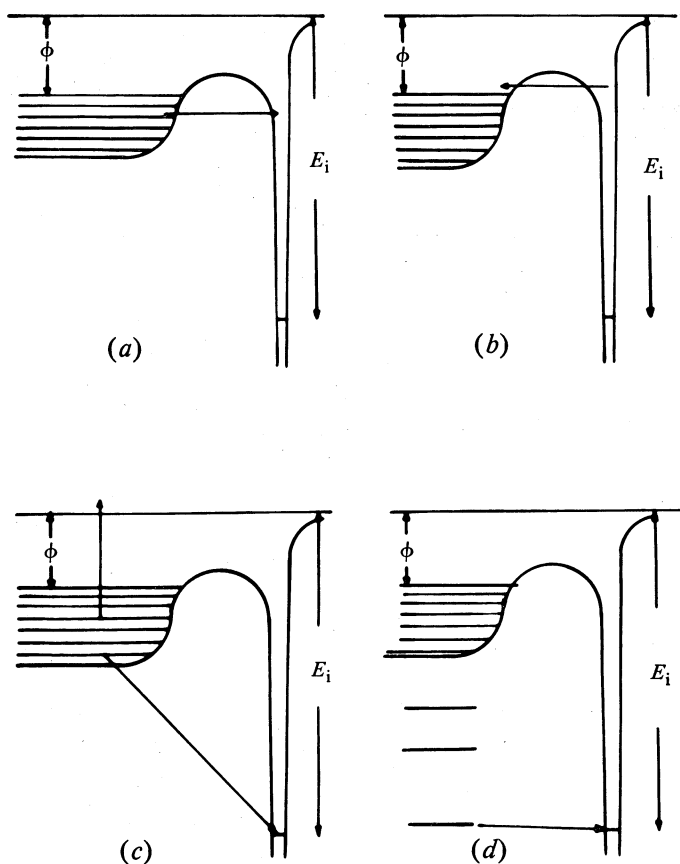

Fig. 5. Schematic diagrams of the types of Auger and resonance electron exchange processes believed to contribute to neutralization of scattered ions (Hagstrum 1954): (a) resonance neutralization; (b) resonance ionization; (c) Auger neutralization; (d) quasi-resonant neutralization.

Auger type electron exchange events between the ion (or atom) close to the surface. These exchange processes are fast, with typical transition rates of 10^{16} s^{-1} for resonance processes and 10^{14} s^{-1} for Auger processes. Hagstrum (1977) has developed a theoretical model for these exchange processes, predicting that the probability P of the particle surviving in its ionized state at large distances from the surface is of the form

$$P = \exp(-a/v_\perp),\tag{6}$$

where a is a constant involving the transition rate at the surface and distances characteristic of the exchange process, and $v_\perp$ is the perpendicular component of particle velocity away from the surface. Other types of neutralization are known to occur.

The differential cross section for scattering is a steadily decreasing function of increasing energy, while the probability of survival of the charged state is, from equation (6), a steadily increasing function of the energy of the scattered ion. The net result of the two processes is an ion yield at a given scattering angle which increases steadily at low energies, reaches a peak and then decreases steadily with further
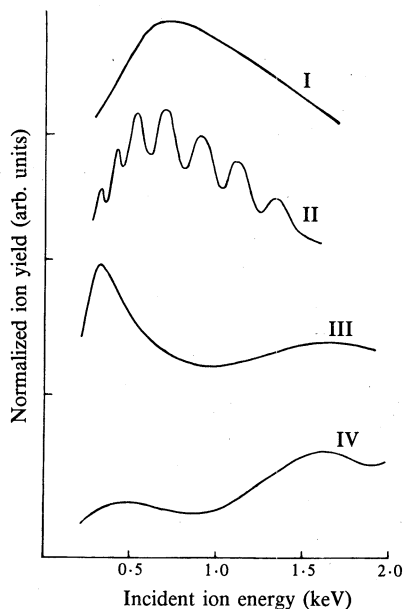

Fig. 6. Schematic representation of the four general types of neutralization behaviour identified by Rusch and Erikson (1977) (see text).
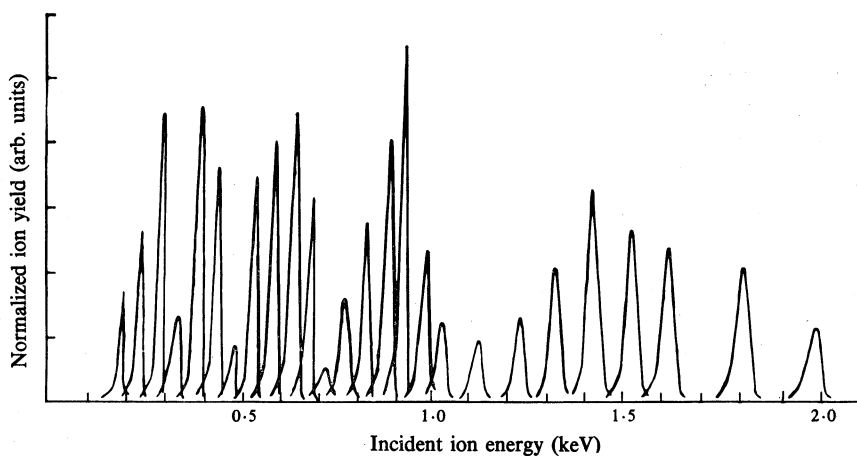

Fig. 7. Experimental results for the variation of normalized ion yield as a function of ion energy for He$^+$ on Pb at $\theta = 90°$ (R. J. MacDonald and G. C. Chapman, unpublished data).

increasing energy. Such a behaviour is observed, but not in all cases. Rusch and Erikson (1977) have identified four distinct types of variation of the ion yield with increasing incident ion energy; these are shown schematically in Fig. 6. The case I approximates closest to the case mentioned above, that of competing cross section

and survival probability of the type described by equation (6). The other types of behaviour II–IV are most likely associated with different neutralization processes.

The behaviour illustrated by class II and characterized by relatively rapid oscillations in the ion yield as a function of energy, and hence in the neutralization probability as a function of energy, is shown in detail in Fig. 7 for the case of He^+ incident on Pb. This behaviour has been identified as the result of a quasi-resonant charge exchange between the ground state of the He atom and the inner 5d orbital of Pb in the solid. According to the model of Lichten (1965), a quasi-molecule is formed in the collision and, depending on the time spent in this quasi-molecular state relative to the orbital period of the shared electron, the shared electron may or may not be captured by the He^+ emerging from the collision. Quantum mechanical phase interference between the two states leads to the oscillatory differential charge transfer cross section Q being of the form (Tully and Tolk 1977)

$$Q = Q(p,v) = A_1(p,v) + A_2(p,v)\sin^2(\beta/\hbar - \delta), \tag{7}$$

where p is the impact parameter, v the relative velocity between the colliding particles, A_1 a non-oscillatory term, A_2 the amplitude factor and δ the phase factor. Further,

$$\beta = \int_{r_0}^{\infty} \{\Delta E(r)/v(r)\} \, dr, \tag{8}$$

where r_0 is the distance of closest approach and $E(r)$ the energy separation between the two states. For small scattering angles, $v(r)$ is approximately constant so that

$$\beta = v^{-1} \int_0^{\infty} \Delta E(r) \, dr = \langle E_r \rangle/v, \tag{9a}$$

$$Q(p,v) = A_1(p,v) + A_2(p,v)\sin^2(\langle E_r \rangle/\hbar v - \delta). \tag{9b}$$

This implies the period of oscillations will be uniform when the yield is plotted as a function of $1/v$, and this behaviour has been observed (Rusch and Erikson 1977). The model also suggests that the oscillations in the neutralization behaviour are due mainly to the binary collision event (and not to interaction with the surface as a whole). Similar oscillations are observed in gas-phase collision work (Zartner *et al.* 1978). In solids the combinations involving He^+ can be predicted by plotting the energies of the atomic states of the target atoms; oscillatory structure is observed in all cases involving quasi-resonance (within ± 10 eV) of an inner level of the atom of the solid, and the ground state of He. This is shown in Fig. 8.

The oscillations in the ion yield can be Fourier analysed (Rusch and Erikson 1977). Such analysis indicates several components to the oscillations, which suggests competing neutralizing events. It is not possible as yet to determine the validity of this statement, but recent experiments testing the possibility of a quasi-resonant exchange to excited states of the He atom (in the case of He^+ scattered off Pb) found no evidence for this as a possible contribution (Taglauer *et al.* 1980). Further, the oscillatory behaviour observed shows differences depending on the chemical environment of the atom involved in the quasi-resonant exchange. It is obvious that our understanding is still limited.

The remaining two cases identified by Rusch and Erikson (1977), cases III and IV in Fig. 6, have not been studied in detail and the processes contributing to their particular behaviour have not been identified.

If the trajectory of the incident ion is taken into account, the ion may be neutralized on the incoming trajectory, during the collision event or on the exit trajectory. In general it is not possible to separate these contributions except by a process of fitting experimental results to theoretical equations. For example, Brongersma *et al.* (1976) suggested the neutralization factor could be written

$$P = \exp\left[-\left\{\frac{b}{v} + a\left(\frac{1}{v_i} + \frac{1}{v_f}\right)\right\}\right],\tag{10}$$

where v is the c. m. velocity and v_i, v_f are the incoming and outgoing normal components of the ion velocity. The term b/v accounts for the collisional contribution, while a/v_i and a/v_f account for the incoming and outgoing contributions respectively.
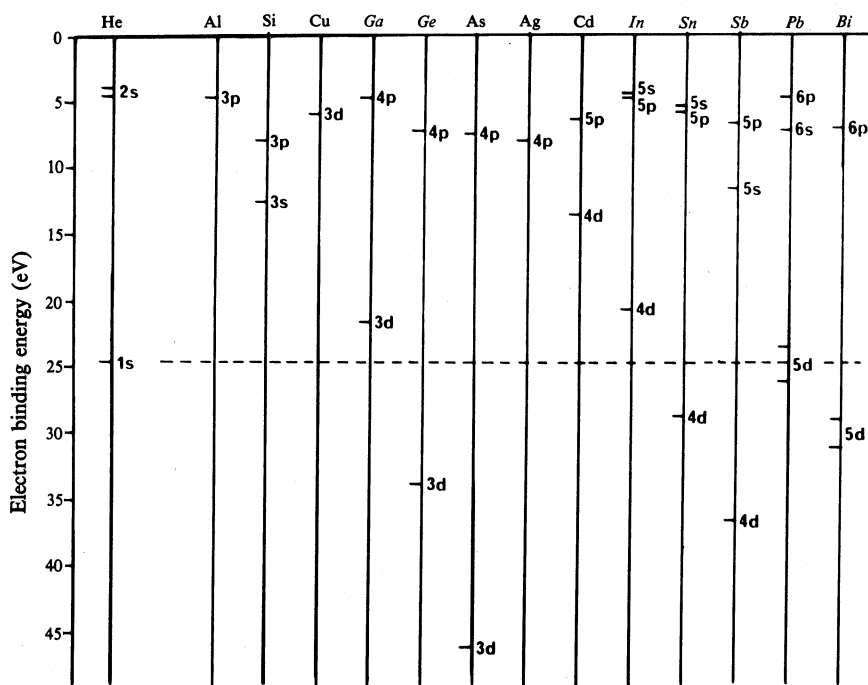

Fig. 8. Quasi-resonance behaviour of the ground state of He atoms with several different target materials (Heiland and Taglauer 1976). Elements in italics represent those exhibiting oscillatory behaviour in the ion yield.

Verheij *et al.* (1976) have analysed a similar situation in considerably more detail. An overall variation of ion yield with a parameter such as energy, angle of incidence or angle of exit is then fitted by an equation similar to or more complex than equation (10). It is extremely difficult to extract from this the individual contributions. However, using an ion scattering apparatus capable of angular resolved measurements in three dimensions, we can attempt experiments of the type shown schematically in Fig. 9. The incoming trajectory and impact parameter (and hence collisional contribution) can be maintained constant while the outgoing trajectory may be varied by moving the analyser in a plane normal to the plane of the incident beam and normal

to the surface. This will differentiate the outgoing contribution. A similar experiment can then differentiate the incoming contribution. By varying the energy (or impact parameter) the collisional contribution can be defined.

4. Applications of Ion Surface Scattering

The energy of the scattered ion at a given scattering angle is, from equation (1), dependent on the mass ratio of incident to struck particle. From the energy spectrum, the identification of surface constituents is possible. The spectrum however is complicated by the close but regular array of scattering centres about the given atom. In Fig. 10 some of the possible scattering events giving rise to a typical spectrum are shown. This highlights the two possible types of measurements—the one related to constituents on the surface, the other to the arrangement of atoms about the scattering event, i.e. surface crystallography. A third group of experiments is related to the basic scattering event, and neutralization processes involved in that event.
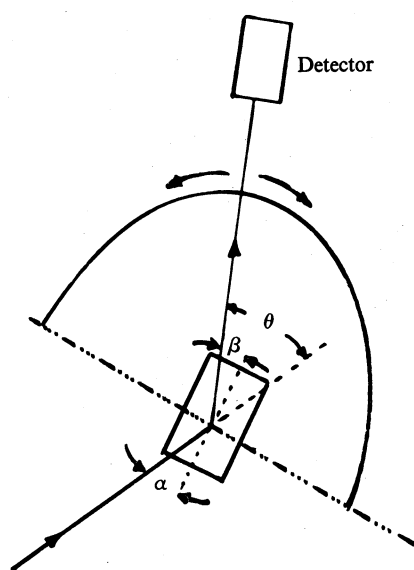

Fig. 9. Schematic representation of an experiment to differentiate the three components of neutralization along the ion trajectory.

Consider first the multiple scattering processes of which the double scattering event C in Fig. 10 is an example. These are multiple scattering events in that the net scattering angle is the result of a sequence of collisions between the incident ion and closely spaced atoms on the surface. Thus, peak C in Fig. 10 is the result of a sequence of two collisions, each a relatively small angle collision, but summing to the larger angle scattering through the angle θ. In general this gives rise to a peak at a higher energy than the single scattering peak B, but whose energy shift from B is a function of the distance between the contributing collisions. In a polycrystalline surface the distribution of interatomic spacings broadens the double scattering peak to a shoulder on the high energy side of the single scattering peak. In a single crystal the double scattering peak is sharply defined and shifts with crystallographic direction.

The scattering of this type is complex but can be quite accurately represented by scattering from a chain of atoms (Kivrilis *et al.* 1966). The important point is that as the angle of incidence to the chain, measured from the surface, is decreased the
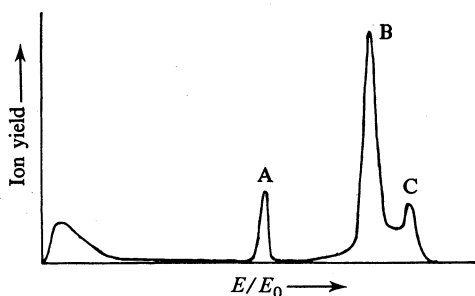
Fig. 10. Schematic representation of several possible scattering events identifiable in low energy ion scattering:

A, a binary collision with an adsorbed impurity;

B, a binary collision with a target atom;

C, a double scattering event involving two sequential collisions with target atoms.
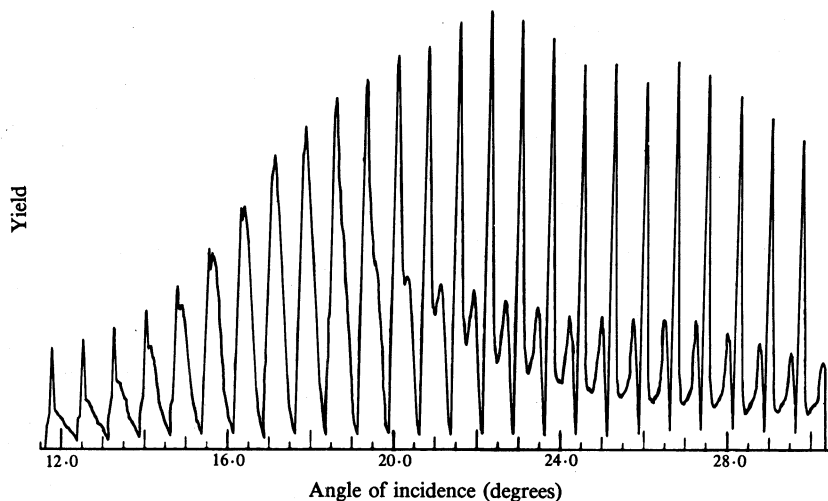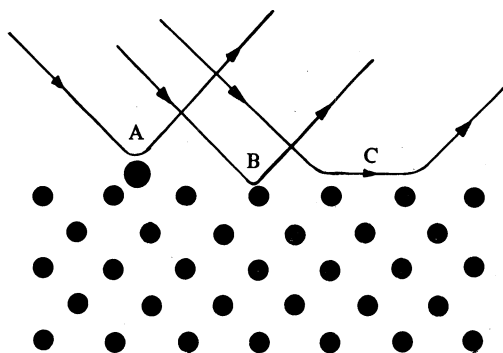

Fig. 11. Demonstration of the variation of separation in energy of the single and double scattering peaks as the angle of incidence to the surface is decreased for 6 keV Ar^+ incident in a W $\langle 100 \rangle$ direction (O'Connor 1978). The total scattering angle is $\theta = 60°$.

energy difference between the single and double scattering peaks decreases until they merge. This is partly due to the incoming ion beginning to interact with the ion in front of the one responsible for the single scattering. The net result of this is that if the position of the two peaks as a function of angle of incidence to the surface is

plotted, an 'energy–angle' loop results. This is usually done by computer simulation of the event. The experimental effect is demonstrated in Fig. 11, in which the scattering of a 6 keV Ar$^+$ beam off the W $\langle 100 \rangle$ direction is shown as a function of the angle of incidence to this direction. In Fig. 12 the position of the single and double scattering peak as a function of angle of incidence to the chain, determined by computer simulation of the scattering event, is shown for different directions in the single crystal surface.
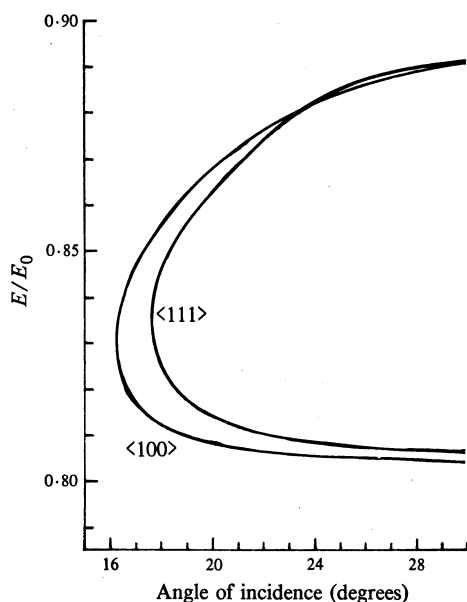

Fig. 12. Results of computer simulation of the scattering from a chain of atoms. The positions of the single and double scattering peaks are plotted as a function of the angle of incidence measured to the surface. The effect of different spacing in the different crystal directions is shown for the case of 10 keV Ar$^+$ incident on a W (110) surface. The total scattering angle is $\theta = 60°$.

Studies in Surface Crystallography using Double Scattering Events: W (110)

Fig. 12 shows that the behaviour of the energy–angle loop depends on the interatomic spacing—thus it can be used for crystallographic studies, particularly of the surface crystallography. In the experiment, the energy of the scattered ions was scanned over the interval containing the single and double scattering peaks. The target was rotated about the surface normal, an energy spectrum being collected at each angular setting. The system was automated. One set of angular scans was obtained at each of a range of angles of incidence, for a constant scattering angle. By observing where $E–\alpha$ loops close, as in Fig. 11, the corresponding crystallographic direction can be identified. The deviation of this direction from that predicted from the bulk structure gives a measure of the surface relaxation in the surface plane. Thus the W (110) surface was shown to have less than 2% relaxation in the surface plane (O'Connor 1978; O'Connor and MacDonald 1980). No comment on the relaxation into the crystal was possible from these measurements.

Inferences on the Interaction Potential from Ion Surface Scattering

Fig. 12 shows the $E–\alpha$ loop to be dependent on spacing in the atomic chain. Fig. 13a shows that for a given atomic chain, the simulation predictions depend on the interatomic potential assumed to operate. Comparison with experiment allows inference to be made regarding the correct potential function to use. In Fig. 13a we compare

some experimental results with simulations using a frozen lattice chain. In practice the lattice chain is subject to thermal vibrations, and the effect of these can be simulated, yielding the results in Fig. 13*b*. The loop no longer closes and the single scattering peak does not disappear as the frozen lattice simulation would suggest. This is nearer the experimental situation (Fig. 11). Fig. 13*b* shows also the comparison of experimental results with simulations including the thermal vibrations derived from different potentials (O'Connor 1978).
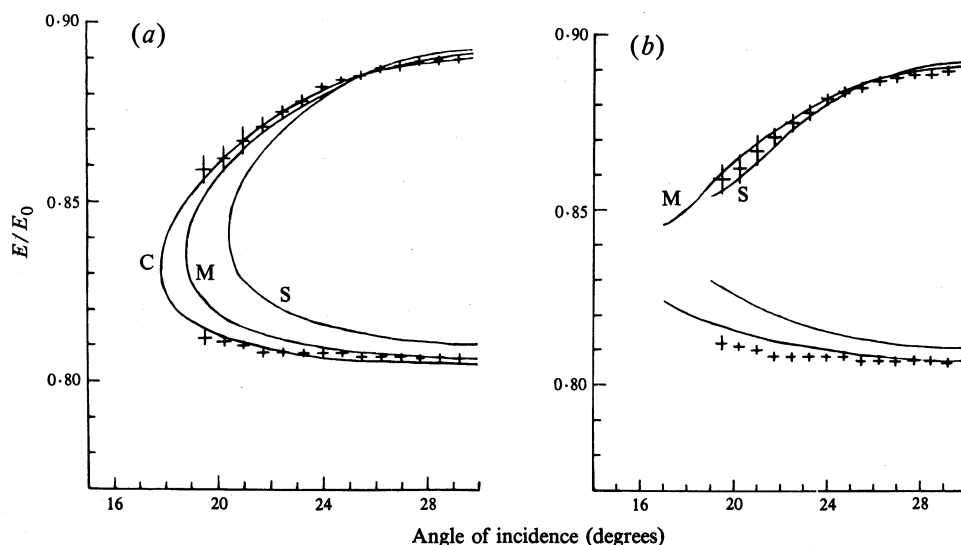

Fig. 13. Comparison of experimental results (crosses) with computer simulations of (*a*) the E–α loop for a frozen lattice and (*b*) the E–α loop including thermal vibrations. The effect of different forms of the screened potential is shown for 6 keV Ar^+ scattered off the $\langle 100 \rangle$ chain in a W (110) surface. The potentials used are (after O'Connor 1978): C, Csavinsky; M, Moliere (Torrens 1972); S, modified Moliere (O'Connor and MacDonald 1977). The total scattering angle is $\theta = 60°$.

Studies of the Neutralization Behaviour of Scattered Ions

It is obvious that quantitative analysis using low energy ion scattering spectroscopy demands an understanding of neutralization behaviour. In Section 3 above, an experiment currently underway to study neutralization events was described. There are a variety of other experiments which can provide some information. For example, a measurement of the ion yield as a function of energy showed the oscillatory behaviour exemplified by the case of He^+ on Pb. For a system such as He^+ incident on Ni or Mo, case I of the Rusch and Erikson (1977) categorization applies and the ion yield is apparently determined only by the exit of the ion from the surface. According to equation (6), a plot of $\ln(I/I_0)$ as a function of $(I/v_\perp)$ should then yield a straight line whose slope gives the transition rate constant (survival coefficient) a. This is shown for the case of 90° scattering of He^+ off Ni and Mo in Fig. 14. The yields shown have been reduced by the ion beam density and the scattering cross section. The fit to the straight line is quite good, the survival coefficient being $3 \cdot 44 \times 10^6$ and $4 \cdot 16 \times 10^6$ m s^{-1} for Ni and Mo respectively. These values suggest the electron exchange event is likely to be a resonance transfer process.
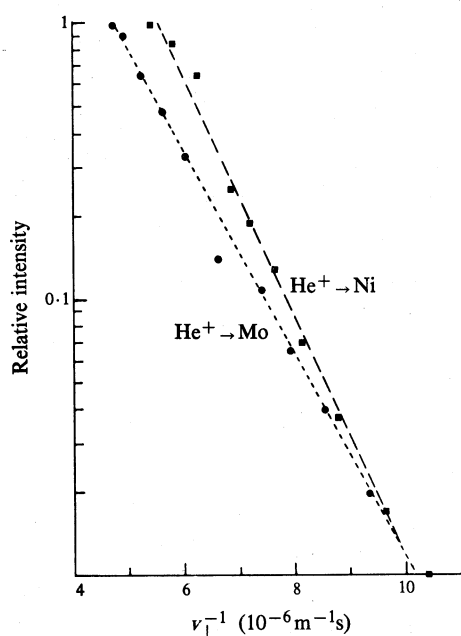
Fig. 14. Plot of ln(relative intensity) as a function of $v_{\perp}^{-1}$ for He^+ scattered off Ni and Mo at a scattering angle of 90°. The relative intensity values are corrected for beam current density variations and for changes in the differential cross section for scattering (Moliere potential).
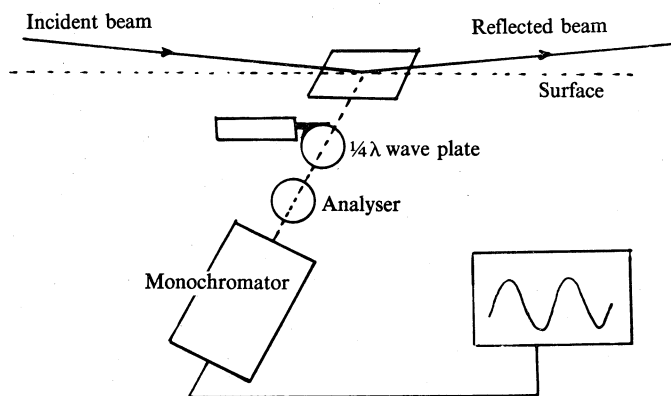

Fig. 15. Experimental arrangement for the study of polarization of photons emitted from excited atoms formed by neutralization of ions at grazing incidence to a surface.

Experiments related to the neutralization process can involve studies of the neutralized particle rather than the scattered ion, particularly when the neutralization involves an electron in an excited state of the atom. Photon emission can then be studied. One group of interesting experiments in which we have been involved concerns studies of the polarized emission from atoms formed as a result of neutralization of an ion incident on a surface during the scattering event (Andra *et al.* 1977). These experiments were performed in the apparatus shown schematically in Fig. 15 (Martin *et al.* 1980). The ions, in this case H_2^+ at 50 keV, were directed at grazing incidence on an Nb target and the polarization was measured by a system involving a rotating quarter-wave plate, located at right angles to the beam direction. From

the intensity as a function of the angle of rotation of the $\frac{1}{4}\lambda$ plate, the reduced Stokes parameters defining the degree of polarization can be studied. These results for the Balmer lines are shown in Fig. 16. A pure 2θ oscillation in intensity is indicative of a high degree of circular polarization, while a more complex pattern indicates the presence of linearly polarized components.
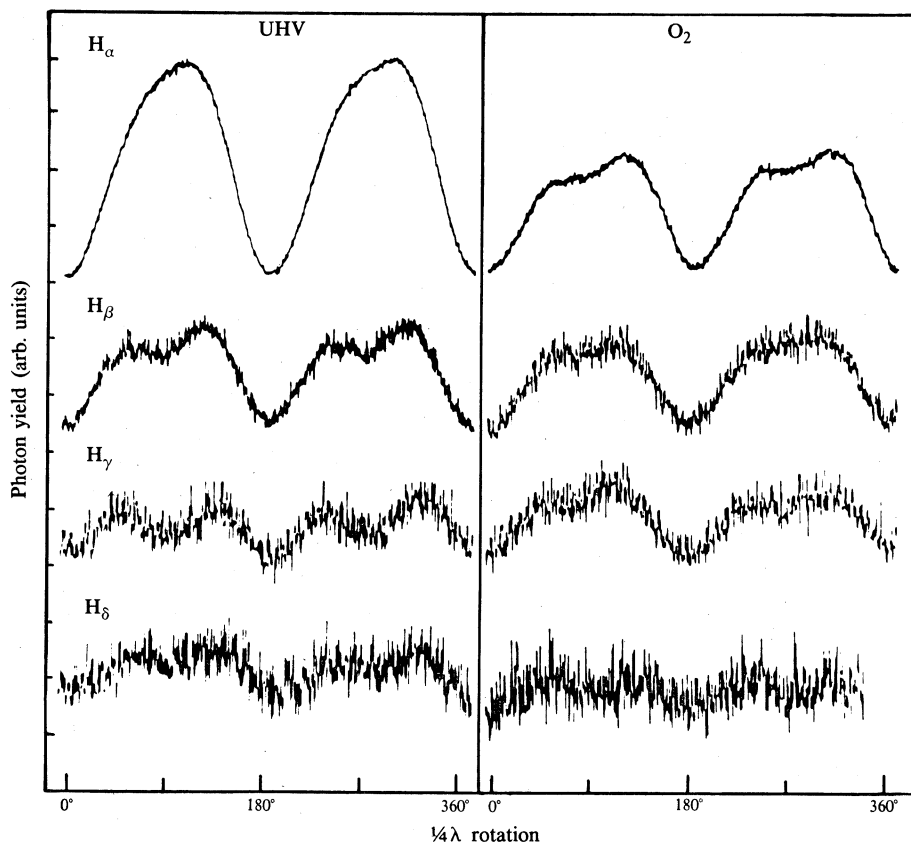

Fig. 16. Intensity variations in the emission as a function of the angle of rotation of the $\frac{1}{4}\lambda$ plate. These data are for the case of H_2^+ incident at 50 keV on an Nb surface. Measurements were made under UHV (10^{-9} torr) and O_2 contaminated (10^{-5} torr) conditions (Martin *et al.* 1980). (Note: 1 torr = 133 Pa.)

In some respects the most interesting result is the dependence of the degree of circular polarization on the level of surface contamination. This is demonstrated in Fig. 17, which shows the S/I value plotted as a function of the background partial pressure of oxygen. The full curve represents a fit to these experimental results, assuming that the degree of surface polarization is directly proportional to the extent of surface coverage with adsorbed oxygen. This coverage is determined by an equilibrium between rate of adsorption from the background and rate of desorption due to sputtering of the adsorbed gas.

These results are difficult to interpret as yet in terms of the neutralization of the incident H_2^+. It has been suggested (Tolk *et al.* 1978) that the circular polarization is the result of preferential capture into one state of particular magnetic quantum number.

However, the origin of the linear polarization at higher excitation levels is not under-stood. Polarization events in gas-phase scattering are themselves difficult to interpret and calculate theoretically, but the difficulty increases when the complexity of electron distributions in the solid has to be built in. Comparative experiments involving gas-phase and surface collisions may contribute to our knowledge of neutralization events.
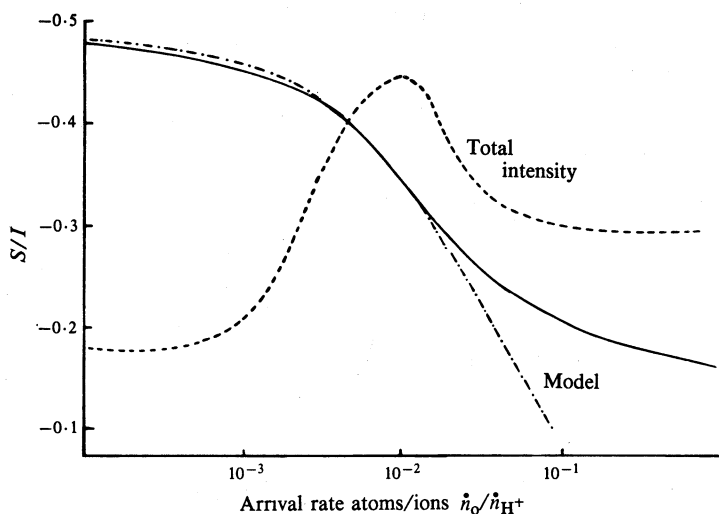

Fig. 17. Variation of the reduced Stokes parameter S/I for circular polarization as a function of the pressure of O_2 in the background gas (Martin *et al.* 1980). The full curve is drawn through experimental points, the dashed curve is the variation in total intensity and the dot–dash curve represents a model fit, assuming S/I is proportional to surface coverage of O_2.

5. Conclusions

This paper has concentrated on ion–surface scattering spectrometry and the type of work that was done at the ANU. The physical processes involved are extremely complex and it is not possible to readily do quantitative analysis with this technique. The experimenter is plagued with uncertainties regarding the neutralization processes possible, and has to deal with uncertainties in the scattering potential involved. These remarks apply mainly to the low energy regime of the experiments. The scattering of ions from a surface however can be used in a number of ways to provide good experimental data. Thus we quote the surface crystallography measurements here and refer to a wide variety of adsorption studies in the literature (see e.g. MacDonald *et al.* 1980). In addition there is some extremely interesting physics to be studied which has bearing on the quantitative analysis potential of ion–surface scattering.

Acknowledgments

References

Andra, H. J., Frohling, R., and Plohn, H. J. (1977). *In* 'Inelastic Ion–Surface Collisions' (Eds N. H. Tolk *et al.*) (Academic: New York).

Bhattacharya, R. S., Eckstein, W., and Verbeek, H. (1980). *Surf. Sci.* **93**, 563.

Brongersma, H. H., Hazewindus, N., van Niewland, J. M., Otten, A. M. M., and Smets, A. J. (1976). *J. Vac. Sci. Technol.* **13**, 670.

Cobas, A., and Lamb, W. E. (1944). *Phys. Rev.* **65**, 327.

Hagstrum, H. D. (1954). *Phys. Rev.* **96**, 325.

Hagstrum, H. D. (1977). *In* 'Inelastic Ion–Surface Collisions' (Eds N. H. Tolk *et al.*) (Academic: New York).

Heiland, W., and Taglauer, E. (1976). *Nucl. Instrum. Methods* **132**, 535.

Kivrilis, V. M., Parilis, E. S., and Turaev, N. Yu. (1966). *Dokl. Akad. Nauk SSSR* **173**, 805.

Lichten, W. (1965). *Phys. Rev.* **139**, A27.

Luitjens, S. B., Algra, A. J., Suurmeijer, E. P. Th. M., and Boers, A. L. (1980). *Appl. Phys.* **21**, 205.

MacDonald, R. J., Taglauer, E., and Heiland, W. (1980). *Appl. Surf. Sci.* **5**, 197.

Martin, P. J., Berzins, L., and MacDonald, R. J. (1980). *Surf. Sci.* **95**, L277.

Massey, H. S. W. (1930). *Proc. Cambridge Philos. Soc.* **26**, 386.

O'Connor, D. J. (1978). Ph.D. Thesis, Australian National University.

O'Connor, D. J., and MacDonald, R. J. (1977). *Radiat. Eff.* **34**, 247.

O'Connor, D. J., and MacDonald, R. J. (1980). *Radiat. Eff.* **45**, 205.

Rusch, T. W., and Erikson, R. L. (1977). *In* 'Inelastic Ion–Surface Collisions' (Eds N. H. Tolk *et al.*) (Academic: New York).

Shekhter, S. S. (1937). *Zh. Eksp. Teor. Fiz.* **7**, 750.

Taglauer, E., Heiland, W., MacDonald, R. J., and Tolk, W. H. (1980). *J. Phys.* B **12**, L533.

Tolk, N. H., Tully, J. C., Kraus, J. S., Heiland, W., and Neff, S. H. (1978). *Phys. Rev. Lett.* **41**, 643.

Torrens, I. M. (1972). 'Interatomic Potentials' (Academic: New York).

Tully, J. C., and Tolk, N. H. (1977). *In* 'Inelastic Ion–Surface Collisions' (Eds N. H. Tolk *et al.*) (Academic: New York).

Verheij, L. K., Poelsma, B., and Boers, A. L. (1976). *Nucl. Instrum. Methods* **132**, 559.

Zartner, A., Taglauer, E., and Heiland, W. (1978). *Phys. Rev. Lett.* **40**, 1259.